J Electroceram (2011) 27:1–6
DOI 10.1007/s10832-009-9566-y

Development of piezoelectric actuators for active X-ray optics

Dou Zhang · Daniel Rodriguez-Sanmartin · Tim W. Button · Carolyn Atkins · David Brooks · Peter Doel · Camelia Dunare · Charlotte Feldman · Ady James · Alan Michette · William Parkes · Slawka Pfauntsch · Shahin Sahraei · Tom Stevenson · Hongchang Wang · Richard Willingale

Received: 19 September 2008 / Accepted: 4 March 2009 / Published online: 21 March 2009

Abstract Piezoelectric actuators are widely utilised in adaptive optics to enable mirrors having an actively controlled reflective surface for the purpose of the wavefront correction by reducing the effects of rapidly changing optical distortion. Two new prototype adaptive X-ray optical systems are under development with the aim of approaching the fundamental diffraction limit. One proposed technology is microstructured optical arrays (MOAs) involving two or four piezoelectric strips bonded to a silicon wafer to produce a micro-focused X-ray source for biological applications, and which uses grazing incidence reflection through consecutive aligned arrays of channels obtained using deep silicon etching. Another technology is large scale optics which uses a thin shell mirror bonded with 20–40 piezoelectric actuators for the next generation of X-ray telescopes with an aim to achieve a resolution greater than that currently available by Chandra (0.5"). PZT-based piezoelectric actuators are being developed in this programme according to the design and implementation of the proposed mirror and array structures. Viscous plastic processing is chosen for the preparation of the materials system, which is subsequently formed and shaped into the suitable configurations. Precise controls on the thickness, surface finish and the curvature are the key factors to delivering satisfactory actuators. Unimorph type piezoelectric actuators have been proposed for the applications and results are presented regarding the fabrication and characterisation of such piezo-actuators, as well as the related design concepts and comparison to modelling work.

Keywords Piezoelectric · Actuator · X-ray optics

D. Zhang (✉) · D. Rodriguez-Sanmartin · T. W. Button
School of Metallurgy and Materials, University of Birmingham,
Edgbaston,
Birmingham B15 2TT, UK
e-mail: d.zhang.1@bham.ac.uk

C. Atkins · D. Brooks · P. Doel · H. Wang
Department of Physics and Astronomy,
University College London,
Gower Street,
London WC1E 6BT, UK

C. Dunare · W. Parkes · T. Stevenson
Scottish Microelectronics Centre,
School of Engineering and Electronics, University of Edinburgh,
West Mains Road,
Edinburgh EH9 3JF, UK

C. Feldman · R. Willingale
Department of Physics and Astronomy, University of Leicester,
Leicester LE1 7RH, UK

A. James
Mullard Space Science Laboratory, University College London,
Holmbury St. Mary, Dorking,
Surrey RH5 6NT, UK

A. Michette · S. Pfauntsch · S. Sahraei
Department of Physics, King's College London,
Strand,
London WC2R 2LS, UK

1 Introduction

Adaptive optics plays a significant role in a number of optical instruments for the correction of wave aberrations. Deformable mirrors (DM) are the key component in reducing the effects of rapidly changing optical distortion by the adjustment of the curvature, which can be achieved by applying a mechanical bending momentum through a

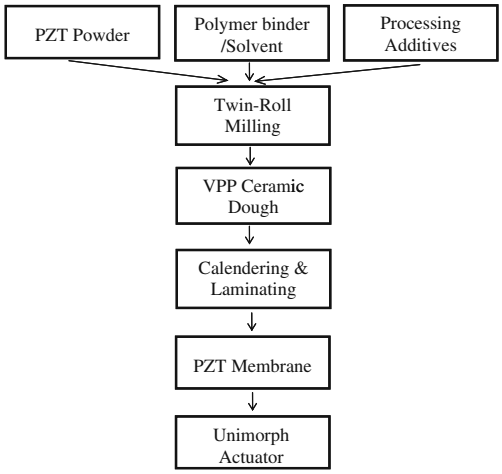

Fig. 1 Flow chart of the fabrication of PZT membrane and actuator by using a VPP process

range of actuation techniques, such as electrostatic actuation [1]. Piezoelectric actuators are especially appealing due to the ability of offering large amplitude continuous deformations with high speed and low voltage[2].

Recently, lead zirconium titanate (PZT) thin films prepared by sol-gel deposition have been developed for the unimorph microactuator in silicon continuous-membrane DM by using a micromachining process [3]. Typical transverse piezoelectric coefficient d_{31} of PZT thin films are in the range of 10–40 pC/N, [4, 5] which are much lower than the bulk value around 100–300 pC/N [6]. Such thin films type actuators normally achieve displacements of a few microns [3]. When a larger stroke i.e. tens of microns displacement is required, and in order to maintain the best thickness ratio between the mirror membrane and PZT films, thicker PZT films become necessary and can be conveniently fabricated by the screen printing [7] and electrophoretic deposition methods [8]. However, thick films generally suffer from issues [9] including the interfacial reaction with the substrate and the electrode, constrained shrinkage, and porous microstructures. In order to take advantage of a d_{31} coefficient as close to the bulk value as possible and achieve larger driving force, PZT thick films have been prepared by a thinning process from bulk ceramics using a wet-etching method for a MEMS deformable mirror application [10].

In this paper, PZT membranes with controlled surface finish and thickness were fabricated by a viscous plastic process (VPP) technique [11]. VPP process generally provides improved material properties compared to conventional dry powder pressing and slip casting due to its capability of breaking down the agglomerates even in high solids loading paste system [12]. Good plasticity in the green state facilitates complex shaping processes and the control of membrane thickness, i.e. 50–200 μm in this study. Unlike conventional thick film processes requiring a substrate to enable the printing and sintering, the membrane obtained via the VPP process is discrete and free-standing, which, therefore, can deliver density and piezoelectric properties similar to the bulk values, and offers the flexibility of curving the membrane to the required radius of curvature. Compared to thinning using etching, the VPP process is limited in obtaining thicknesses below 50 μm but has the advantage of simplicity.

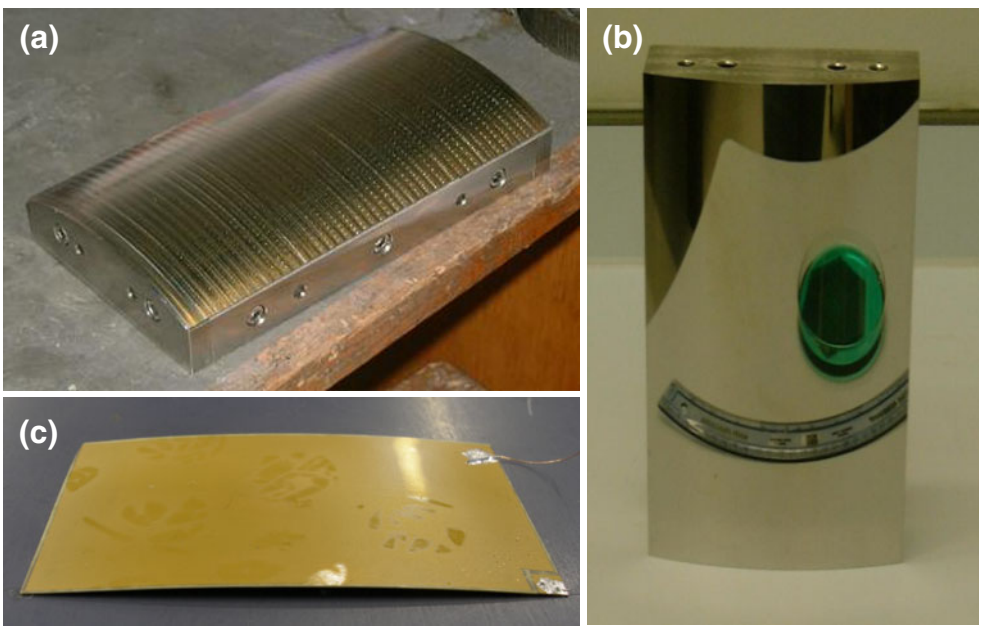

Fig. 2 Photos of (**a**) a milled cylindrical mandrel with dimensions of 100×200×40 mm^3; (**b**) the cylindrical mandrel after polishing; (**c**) a curved PZT unimorph actuator with dimensions of 17×33×0.15 mm^3

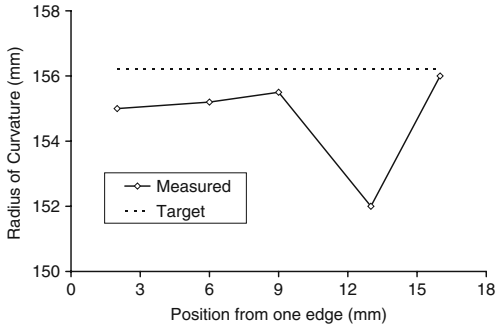

Fig. 3 The targeted and measured ROC of a PZT curved membrane. The ROC was measured by a profilometer (Talysurf) and the position indicates the distance from one edge along the width of the membrane

Two new prototype adaptive X-ray optic systems are under development with the aim of approaching the fundamental diffraction limit. One proposed technology is microstructured optical arrays (MOAs) involving two or four piezoelectric strips bonded to a 10 mm×20 mm silicon chip to produce a micro-focused X-ray source for biological applications, and which uses grazing incidence reflection through consecutive aligned arrays of channels obtained using deep silicon etching [13]. The other interest is actively deformable mirrors in large scale optics for the next generation of X-ray telescopes with an aim to achieve a spatial resolution greater than that currently available by Chandra (0.5") whilst having a high throughput. The initial design is based on a thin nickel shell with an X-ray reflective coating, on the back of which will be bonded a series of piezoelectric actuators [14, 15].

2 Experimental

AVPP process has been utilised in this study to prepare the PZT membranes, as shown in Fig. 1. PZT powders (TRS610C, TRS Technologies, Inc., USA) were mixed with the polymer binder, polyvinyl butyral (PVB), solvent and plasticisers and twin-roll milled to obtain the dough. The details of the general fabrication procedure of VPP method are described elsewhere [11, 16]. The VPP ceramic dough was shaped into membranes with controlled thickness using a calendering and laminating process. The green membranes were then subjected to drying, binder removal, and sintering processes. The sintering was carried out at 1200°C in a controlled PbO-rich atmosphere for 1 h.

After obtaining the sintered membrane, a further precision control on the membrane thickness and the surface finish was performed by a precision lapping machine (Logitech PM5, Glasgow, UK). For the large optics applications, the membranes were reshaped to a controlled curvature by heating on a former. The electrodes were applied by sputtering Cr and Au for 2 and 4 min, respectively.

3 Results and discussion

3.1 PZT unimorph membranes for cylindrical large optics

The prototypes of the thin mirror shell are of 0.4 mm thick and 100 mm wide, and have an overall length of 200 mm for the cylindrical shape and 300 mm for the ellipsoidal shape. An electroforming process is employed to obtain the nickel shell with the support of a polished mandrel. Stainless steel (manufacturing grade 316) was chosen for the cylindrical mandrel production due to high finished surface quality and easy release of the electroformed nickel. Fig. 2(a) and (b) show a 100×200×40 mm^3 stainless steel block before polishing and afterwards, respectively. The average surface roughness of the finished cylindrical mandrel is 4.01 nm measured by a RST500 microscope interferometer.

To minimize the bonding stress which can cause the distortion on the mirror surface and may lead to the fracture of the fragile PZT membrane, a controlled curvature of PZT membrane was required to match the curvature of the nickel shell. The curvature shaping process is carried out after lapping by heating to near the sintering temperature on a former. Fig. 2(c) shows a curved PZT unimorph with dimensions of 33 mm length, 17 mm width and 0.15 mm thickness. The brown colour indicates the Au layer as the electrodes.

The radius of curvature (ROC) of the curved PZT membrane was measured by a Talysurf profilometer along five different positions, and is shown in Fig. 3. The dotted line represents an ideal ROC. The average variation between the measured and targeted ROC is less than 1%, indicating a good match between the PZT membrane and the cylindrical shaped nickel shell.

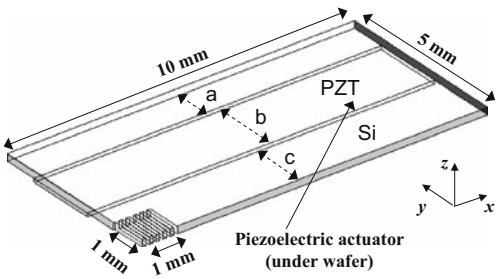

Fig. 4 Schematic geometry of a quarter of a 1D MOA chip, showing the channels array in the central of the silicon wafer and a bonded PZT. The *dashed arrows* indicate variable dimensions, *a*, *b*, and *c*

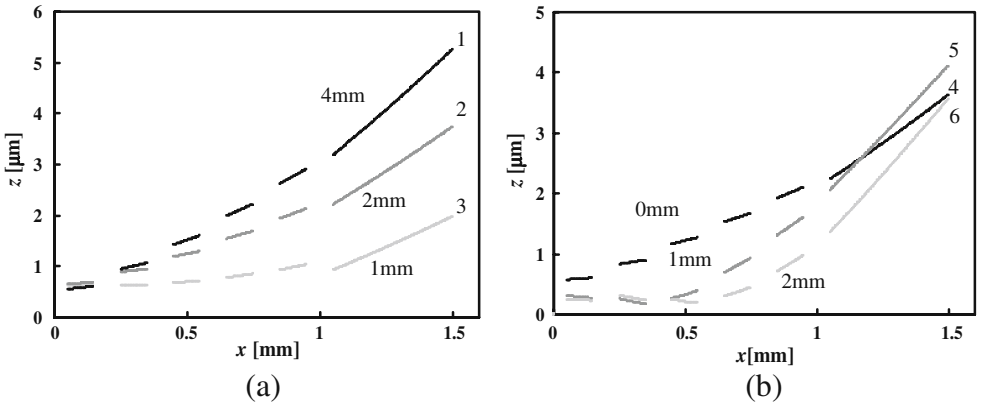

Fig. 5 Simulations of the bending behaviour of a 200 μm thick 1 D MOA actuated by two strips of 100 μm thick PZT-5H. (**a**) Effects of PZT strips width when locating at the centre; (**b**) Effects of the location of 2 mm wide PZT strips relate to the active channel structures. *Curves 1*, *2*, *3*, *4*, *5* and *6* incorporate structural parameters *a*, *b*, and *c* illustrated in Fig. 4

Thirty PZT membranes with ROC of ~155 mm have been made and bonded to the cylindrical shaped nickel mirror shell, and the fabrication of PZT membranes with a mean ROC of 167.5 mm is in progress for the ellipsoidal shaped nickel mirror shell. An optimal bonding process is under investigation at University College London (UCL) at present by using glues having very low shrinkage. Further optical and X-ray focussing tests of such cylindrical and elliptical prototypes will be performed at UCL and the University of Leicester.

3.2 PZT unimorph strips for microstructured optical arrays

Figure 4 shows a schematic geometry of a quarter of a 1D MOA chip with two strips of piezoelectric unimorph actuators. A finite element analysis (FEA) was carried out using the commercial package COMSOL Multiphysics for optimisation of the structural parameters and the configuration of the actuators. Due to the symmetry, only a quarter of the silicon wafer was modelled, thus reducing the processing time and allowing finer FEA meshing. In the simulations, an electric field of 2.5 V/μm was utilised, close to the maximum that these actuators are expected to withstand. The effect of the bonding layer between the actuator and silicon wafer was neglected. PZT-5H was selected in the COMSOL package to provide the piezoelectric properties, due to its similarity to the TRS 610C PZT powders used here.

Figure 5(a) shows the displacement in the *x* and *z* axes when two strips of 100 μm thick actuators were placed in the central region between the edge of the 200 μm thick silicon chip and the active channel structures. The dark curve 1 is for strips of 4 mm width covering the whole area, i.e. a= 0 mm, b=4 mm and c=1 mm. The grey curve 2 is for 2 mm wide strips (a=1 mm, b=2 mm and c=2 mm) and the light curve 3 for 1 mm wide strips (a=1.5 mm, b=1 mm and c= 2.5 mm). After actuating the strip actuators, a bending is generated along the *x*-axis to produce the required curvature for the active channel structures. Bending will also happen along the *y*-axis, but at a much smaller level, due to the high aspect ratio between the length and the width of the strip. As the channel structures exist in the centre of the silicon wafer, the bending results in very complex shapes, and more detailed analyses are still ongoing. The displacement when two strips of actuators of 2 mm width are placed in different locations between the edge of the silicon chip and the active channel structures is shown in Fig. 5(b). The dark curve 4 is for strips adjacent to the active channel structures, i.e. a= 2 mm, b=2 mm and c=1 mm. The grey and light curves are for distances of 1 mm and 2 mm away from the active channel structures, respectively. These simulation results indicate that wider strips and closer location to the active channel structures are preferable for larger displacements. The smallest radius of curvature which can be produced by 4 mm wide strips is ~200 mm. However, in order to achieve a sufficiently short focal length using a double reflection design in which the first component is unbent, the second component would require a radius of curvature of ~50 mm. This may be alleviated by bending both components. Further work is required to find the optimum geometry and the configuration to provide adequate adjustment of the curvatures.

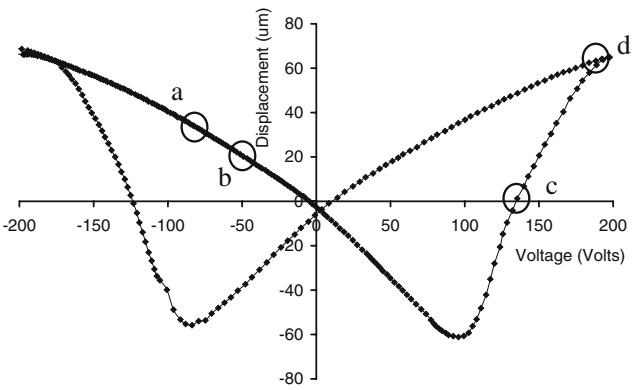

Fig. 6 Correspondence between the displacements and the applied voltages for an MOA test sample. Detailed discussion on four marks along the hysteresis loop *a*, *b*, *c*, and *d* are given in Fig. 7

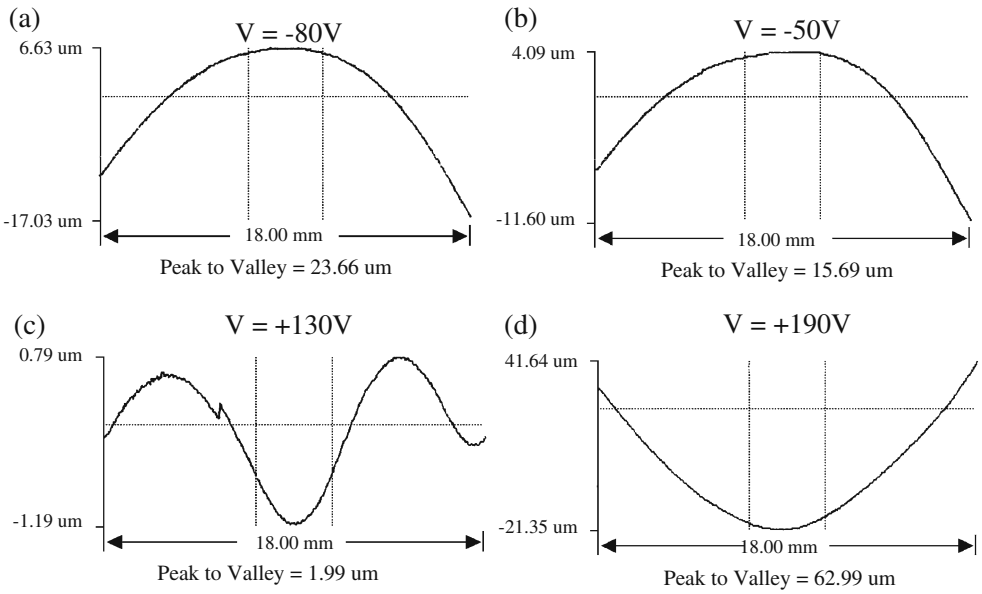

Fig. 7 Scanned displacement along the *x* axis of the MOA chip at four different voltage points in the Butterfly hysteresis cycle using a TalySurf profilometer. The change of applied voltages followed the order of −200 V → −80 V (as shown in (**a**)) → −50 V (as shown in (**b**)) → 130 V (as shown in (**c**)) → 190 V (as shown in (**d**)). **a**, **b**, **c** and **d** are also marked in Fig. 6

Figure 6 shows a complete butterfly loop of the displacements vs. applied DC voltages for an MOA test sample using a ramp of voltage, 4 V/s, with a step of 0.250 V. A 70 μm displacement was obtained at an applied electric field of 1.3 V/μm. Two strips (20 mm×2 mm) of 150 μm thick PZT unimorph were bonded on a 200 μm thick 1 D blank MOA silicon chip (20 mm×10 mm). The test sample has structural parameters a=1 mm, b=2 mm and c=2 mm, corresponding to the curves 2 and 5 in Fig. 5. A laser probe (M5L/2, MEL Mikroelektronik GmbH) was positioned in the geometrical centre of one of the PZT strips for the displacement measurement. The control of the applied voltage and the collection of the laser signals were realised by using a National Instruments PCI-6052E acquisition card based on the Lab View 8.5 system. It is worthy of clarifying that this displacement result reflects the bending across the whole silicon chip, from the geometrical centre to the edge, of 10 mm span, while the simulation results shown in Fig. 5 indicated the displacement only in the channel structure, of 1 mm span. In the view of the curvature of the silicon chip after actuating the PZT strips, 70 μm displacement gives around 714 mm radius of curvature, where the smallest radius of curvature obtained from the simulation is ~200 mm by using 4 mm wide strips, and ~300 mm by using 2 mm wide strips, as shown in Fig. 5. The test results are therefore consistent with the simulation results, considering the difference between the applied electric fields, which are 1.3 V/μm in the test and 2.5 V/μm in the simulation.

Figure 7 shows the displacement profiles along the *x* axis of the MOA chip at four different voltage points in the Butterfly hysteresis loop obtained by a TalySurf profilometer. Curves a, b & d generally show smooth curvatures along the length of the MOA chip at different voltages, indicating the uniformity of the piezo-actuators along the length. Curve c shows a non-uniform response along the length of the MOA chip when the applied voltage increased to 130 V, where the displacement of the MOA chip was close to zero. The non-uniformity is likely due to the transformation of the MOA chip while its shape changed from a negative peak-to-valley to the positive one.

4 Conclusions

PZT based piezoelectric actuators have been developed for smart X-ray mirror applications, namely cylindrical and ellipsoidal shaped large optics and microstructured optical arrays (MOAs). According to the design and implementation of the proposed mirror and array structures, precise controls of the thickness, surface finishing and the curvature of the unimorph actuators have been realised and viscous plastic processing was identified as a suitable method of preparing the materials system and delivering the satisfactory devices. Characterisation and simulation of the bending behaviour of an actuated MOA structure have been obtained and analysed, indicating that the further improvement on the bending performance is necessary by optimising the geometry and the configuration.

Acknowledgements This work is supported by a Basic Technologies Grant from the UK Engineering and Physical Sciences Research Council (EPSRC) (DO4880X). The authors would like to thank the help and advice offered by fellow members of the SXO consortium and especially the technical contributions of Carl Meggs and Geoffrey Dolman.

References

1. T.G. Bifano, R.K. Mali, J.K. Dorton, J. Perreault, N. Vandelli, M. N. Horenstein, D.A. Castanon, Opt. Eng. **36**, 1354 (1997) doi:10.1117/1.601598
2. F. Forbes, F. Roddier, G. Poczulp, C. Pinches, G. Sweeny, R. Dueck, J. Phys. E. Sci. Instrum. **22**, 402 (1989) doi:10.1088/0022-3735/22/6/016
3. Y. Hishinuma, E.H. Yang, J. Microelectromech. Syst. **15**, 370 (2006) doi:10.1109/JMEMS.2006.872229
4. H. Kueppers, T. Leuerer, U. Schnakenberg, W. Mokwa, M. Hoffmann, T. Schneller, U. Boettger, R. Waser, Sens. Actuator A-Phys. **97–98**, 680 (2002) doi:10.1016/S0924-4247(01)00850-0
5. F.F.C. Duval, S.A. Wilson, G. Ensell, N.M.P. Evanno, M.G. Cain, R.W. Whatmore, Sens. Actuator A-Phys. **133**, 35 (2007) doi:10.1016/j.sna.2006.03.035
6. S. Sherrit, H.D. Wiederick, B.K. Mukherjee, Proc. SPIE **3037**, 158 (1997) doi:10.1117/12.271326
7. Y. Jeon, J.S. Chung, K. No, J. Electroceram. **4**, 195 (2000) doi:10.1023/A:1009924113335
8. J. Ma, W. Cheng, J. Am. Ceram. Soc. **85**, 1735 (2002) doi:10.1111/j.1151-2916.2002.tb00344.x
9. R.A. Dorey, R.W. Whatmore, J. Electroceram. **12**, 19 (2004) doi:10.1023/B:JECR.0000033999.74149.a3
10. X.H. Xu, B.Q. Li, Y. Feng, J.R. Chu, J. Micromech. Microeng. **17**, 2439 (2007) doi:10.1088/0960–1317/17/12/008
11. B. Su, D.H. Pearce, T.W. Button, J. Eur. Ceram. Soc. **21**, 2005 (2001) doi:10.1016/S0955-2219(01)00161-3
12. W.J. Clegg, K. Kendall, N.M. Alford, T.W. Button, J.D. Birchall, Nature **347**, 455 (1990) doi:10.1038/347455a0
13. A. Michette, T. Button, C. Dunare, C. Feldman, M. Folkard, D. Hart, C. McFaul, G.R. Morrison, W. Parkes, S. Pfauntsch, A.K. Powell, D. Rodriguez-Sanmartin, S. Sahraei, T. Stevenson, B. Vojnovic, R. Willingaled, D. Zhang, Proc. SPIE **6705**, 670502 (2007) doi:10.1117/12.735500
14. P. Doel, C. Atkins, S. Thompson, D. Brooks, J. Yao, C. Feldman, R. Willingale, T. Button, D. Zhang, A. James, Proc. SPIE **6705**, 67050M (2007) doi:10.1117/12.734608
15. C. Atkins, P. Doel, J. Yao, D. Brooks, S. Thompson, R. Willingale, C. Feldman, T. Button, D. Zhang, A. James, Proc. SPIE **6721**, 67210T (2007) doi:10.1117/12.782955
16. B. Su, T.W. Button, J. Mater. Process. Technol. **209**, 153 (2009) doi:10.1016/j.jmatprotec.2008.01.046